communications physics

A Nature Portfolio journal

Article

https://doi.org/10.1038/s42005-025-02168-0

HydroX, a light dark matter search with hydrogen-doped liquid xenon time projection chambers

W. H. Lippincott[1] ✉, H. N. Nelson[1], D. S. Akerib[2,3], C. Amarasinghe[1], A. Ames[2,3], H. M. Araújo[4], J. W. Bargemann[1], M. C. Carmona-Benitez[5], R. Coronel[2,3], C. E. Dahl[6,7], S. Dey[8], J. Genovesi[5], S. J. Haselschwardt[9], E. Jacquet[4], D. Khaitan[10], D. Kodroff[11], S. Kravitz[12], W. Lorenzon[9], S. Luitz[2,3], A. Manalaysay[11], C. Maupin[13], M. E. Monzani[2,3,14], K. C. Oliver-Mallory[4], E. Perry[11], Y. Qie[10], T. Shutt[2,3], D. J. Temples[7], M. Trask[1], A. Wang[2,3], F. L. H. Wolfs[10], D. Woodward[11], R. Zhang[1] & T. Zhang[11,15]

Experimental efforts searching for dark matter particles over the last few decades have ruled out many candidates led by the new generation of tonne-scale liquid xenon. For light dark matter, hydrogen could be a better target than xenon as it would offer a better kinematic match to the low mass particles. This article describes the HydroX concept, an idea to expand the dark matter sensitivity reach of large liquid xenon detectors by adding hydrogen to the liquid xenon. We discuss the nature of signal generation in liquid xenon to argue that the signal produced at the interaction site by a dark matter–hydrogen interaction could be significantly enhanced over the same interaction on xenon, increasing the sensitivity to the lightest particles. We discuss the technical implications of adding hydrogen to a xenon detector, as well as some background considerations. Finally, we make projections as to the potential sensitivity of a HydroX implementation and discuss next steps.

Astrophysical measurements across all scales from the smallest dwarf galaxies to the cosmic microwave background agree that most of the matter in our universe is made up of dark matter (DM)[1,2]. None of the particles in the Standard Model of particle physics can account for the DM, and the observation of a DM particle would be a revolutionary breakthrough and evidence for new physics. A leading hypothesis for DM is a thermal relic from the Big Bang with a mass between about 1 GeV and 100 TeV, with several candidates predicted by extensions to the Standard Model, often called Weakly Interacting Massive Particles (WIMPs)[1–3]. Candidates can interact via both spin-independent (SI) and spin-dependent (SD) elastic scattering, along with a wider set of more complex interactions that are also important channels for detection[4,5]. To date, no WIMPs have been observed, with a series of experiments setting increasingly stringent limits on the cross section for DM scattering with normal matter. The current best constraint on DM with masses above 10 GeV/c^2 comes from the LZ experiment, a large liquid xenon time projection chamber (LXe-TPC); two other LXe-TPCs, XENONnT and PandaX-4T, have also published strong constraints[6–8].

A largely unexplored window for thermal DM from 10 GeV down to MeV mass scales can be opened up by allowing new force mediators into the theory, below which point constraints from structure formation in the universe take effect. Extensions to the Standard Model produce several electroweak candidates below 1 GeV that evade all constraints from the LHC[9,10]. Other frameworks naturally produce candidates at ~1 GeV, as in Asymmetric Dark Matter[11]. A summary of the case for low mass DM can be found in the 2017 report from the US Cosmic Visions DM working group[12], the 2019 DOE New Initiatives in DM Report[13], and the white papers produced for Snowmass 2021[14–16]. Over the past several years, several experiments have begun probing this region of parameter space via both DM–nucleus and DM–electron scattering, for example, NEWS-G, SENSEI, DAMIC, and SuperCDMS-HVeV as well as XENON, LZ, and DarkSide-50

[1]Department of Physics, University of California, Santa Barbara, Santa Barbara, CA, USA. [2]SLAC National Accelerator Laboratory, Menlo Park, CA, USA. [3]Kavli Institute for Particle Astrophysics and Cosmology, Stanford University, Stanford, CA, USA. [4]Physics Department, Blackett Laboratory, Imperial College London, London, UK. [5]Department of Physics, Pennsylvania State University, University Park, PA, USA. [6]Department of Physics & Astronomy, Northwestern University, Evanston, IL, USA. [7]Fermi National Accelerator Laboratory (FNAL), Batavia, IL, USA. [8]Department of Physics, University of Oxford, Oxford, UK. [9]Randall Laboratory of Physics, University of Michigan, Ann Arbor, MI, USA. [10]Department of Physics and Astronomy, University of Rochester, Rochester, NY, USA. [11]Lawrence Berkeley National Laboratory (LBNL), Berkeley, CA, USA. [12]Department of Physics, University of Texas at Austin, Austin, TX, USA. [13]Sanford Underground Research Facility, South Dakota Science and Technology Authority (SDSTA), Lead, SD, USA. [14]Vatican Observatory, Castel Gandolfo, Vatican City State. [15]Department of Physics, University of California, Berkeley, Berkeley, CA, USA. ✉e-mail: hlippincott@ucsb.edu

through the Migdal effect[17–23]. As for the higher masses, no observations have yet been reported.

For kinematic reasons, low mass DM particles do not transfer energy to heavy nuclei like xenon as efficiently as heavier WIMPs. The smallest DM mass m_χ that a detector with target atomic mass A and nuclear recoil (NR) energy threshold E_{NR} can detect is approximately[12]:

$$m_\chi = 88\ \mathrm{MeV} \times \left[\frac{E_{\mathrm{NR}}}{0.1\ \mathrm{keV}} \times A\right]^{1/2}. \quad (1)$$

For xenon recoils in LXe TPCs, $E_{\mathrm{NR}} \sim 5$ keV for standard conditions, giving sensitivity to ~8 GeV DM particles.

In this article, we discuss HydroX, an idea to deploy hydrogen, the nucleus with the smallest A, into a LXe detector at the level of one percent by number density, providing ~1 kg in a detector the size of LZ. The proton that constitutes the hydrogen nucleus becomes the DM target, with LXe as the sensor. The use of D_2 instead of H_2 can bring neutrons into the interaction. Thus, HydroX can provide sensitivity to both SI and SD channels for both DM–proton and DM–neutron interactions. No other set of target nuclei provides sensitivity to this broad menu of interaction types for DM masses below the proton mass, and, as many DM models predict suppressed leptonic interactions, there is a clear need for experiments designed to detect all possible DM–nucleus interactions at these mass scales.

Methods

LZ as a case study

To study the potential of HydroX, we start by assuming it can be carried out in the LZ detector as described in ref. 24, but most of the arguments can be carried to other detector implementations or a next-generation LXe-TPC[25,26]. LZ consists of a two-phase LXe-TPC containing 7 tonnes of fully active LXe. Xenon is a liquid around 165 K at 1 atmosphere, and the entire inner detector is a cylindrical, cryogenic volume. In a LXe-TPC, particle interactions can create prompt scintillation light, known as S1, and electron–ion pairs. Freed electrons are drifted through the liquid by an electric field perpendicular to the liquid–gas interface, extracted into the gas region, and then accelerated through a stronger electric field, creating proportional scintillation light, known as S2, that is a direct measure of the number of extracted electrons. Photomultiplier tubes (PMTs) collect both S1 and S2 light, with xy position reconstruction provided by the PMT hit pattern of the S2 light, and z reconstruction by the timing between S1 and S2.

The main objective in designing a DM detector is elimination of background radiation that can mimic a DM signal. LZ has been painstakingly constructed out of low radioactivity components in a clean environment to minimize radioactive contamination[27]. Because of the high density of LXe (~3 g/cm^3 at 165 K), external radioactivity is attenuated before it can reach an innermost, "fiducial" volume at the core of a large LXe volume. To further reduce backgrounds, the LZ detector includes two active veto regions outside the main TPC to tag particles generated in detector materials that scatter in the TPC before exiting. LZ and its veto detectors sit in a water tank for further shielding, located in the 4850-foot level of the Sanford Underground Research Facility, in Lead, South Dakota, USA.

Modeling DM–proton scattering in LXe

For sensitivity to galactic DM particles with mass less than 1 GeV, kinematics dictate that the target particle must be light and/or the sensor must have a low energy threshold (see Eq. (1)). As the lightest element, hydrogen being a single proton is kinematically the most attractive nucleus for the detection of NR from sub-GeV DM particles that interact with quarks and/or gluons (the molecular binding energy of H_2 is 4.75 eV, and single proton recoils will be the signal for DM scattering). Less obvious is the potential very low energy threshold in LXe for the detection of a proton recoil. In a LXe-TPC, most of the energy from electronic recoils (ER) is transferred to the electronic system of the medium, producing electronic excitation and ionization (electronic stopping) that lead to S1 and S2. For NR, the recoiling atom primarily experiences quasi-elastic collisions with other xenon atoms

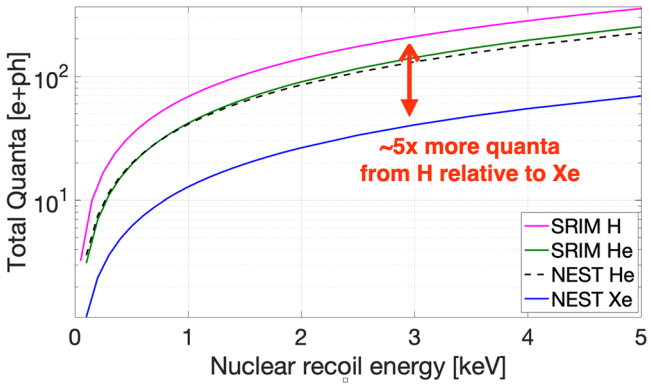

Fig. 1 | Total quanta (photons and electrons) released from various recoils in LXe. The blue curve shows the quanta for low energy Xe recoils in LXe as modeled by NEST. The magenta line shows a SRIM calculation[35] for H recoils, assuming only electronic stopping contributes, with about 5× more quanta produced per unit energy relative to Xe. The green and dashed black lines show two independent predictions for yields from He recoils in LXe, one from SRIM package and the second from NEST. The two models for helium are in good agreement.

mediated by the interatomic potential (nuclear stopping). Energy transferred in these elastic collisions does not produce S1 and S2 signals and is eventually lost to heat, but an inelastic transfer of energy through slow disruption of the xenon electron cloud can occur, producing S1 and S2 with reduced yield and a different S1/S2 ratio compared to ER. Measurements of NR yields in LXe have shown that for energies below 10 keV, less than ~20% of the total xenon recoil energy ends up as visible quanta (photons and electrons). The Noble Element Simulation Technique (NEST) is a widely used, data-driven simulation package that models electron and photon yields in LXe[28–30], and the yellow curve in Fig. 1 shows the total number of quanta released for low energy xenon recoils in LXe as modeled by NEST.

In contrast, a recoiling proton will transfer very little of its energy via elastic collision to xenon atoms, similar to the case of a fast neutron incident on a high-A target, as described by Fermi[31] or Segre[32]. In the limit of hard-sphere proton–xenon collisions, on average only ~1.5% of the proton kinetic energy is lost to xenon kinetic energy per elastic collision; actual proton–xenon collisions are softer than hard sphere, reducing the average energy loss[33]. A typical proton struck by a proton-mass galactic DM particle will survive for at least 100 subsequent elastic proton–xenon collisions prior to falling below the xenon ionization threshold energy (in the hard-sphere limit) with each collision providing an opportunity for excitation of the electrons bound in the xenon atom. By contrast, a typical xenon atom struck by a 100 GeV galactic DM particle will fall beneath the threshold for xenon ionization after an average of only about 8 collisions. Because a proton transfers less of its kinetic energy to translation of the sensor xenon atoms, more of the kinetic energy is available for electronic excitation and ionization, leading to more charge and light production. We estimate the raw electronic and nuclear stopping powers for hydrogen recoils in LXe using the Stopping and Range of Ions in Matter (SRIM) simulation package[34,35], and the predicted signal yield is shown by the magenta curve in Fig. 1 under the assumption that all of the electronic stopping goes into signal but none of the nuclear stopping does. We estimate that H recoils in LXe will result in about five times more quanta released per unit energy relative to Xe recoils.

There are no data measuring yields for H recoils in LXe; there exist measurements for alpha recoils at high energy, for which a similar signal enhancement can be expected[30,36,37]. While the alpha data are taken at MeV-scale energies, the NEST package includes a power-law extrapolation down to low energies[38], shown by the dashed black line in Fig. 1. Our SRIM calculation for a He projectile is shown in green, showing good agreement with the NEST extrapolation, particularly given the different inputs and assumptions made by the two models. This agreement combined with the physical intuition already described gives some confidence in the

expectation that proton recoils will produce significantly more photons and electrons than Xe recoils.

A second key question is how the increased signal is partitioned into S1 and S2 pulses for proton recoils. As the S2:S1 ratio provides event-by-event discrimination between ER and NR signals in a LXe-TPC, it will be crucial to understand whether ER backgrounds will be distinguishable from proton recoils. The number of ionization electrons in an event is determined by a complex interaction of the drift field, the electron thermalization length, and the track density. Electrons and ions can recombine, reducing the number of electrons in favor of scintillation photons. The presence of H_2 might speed up the thermalization process, in principle leading to more recombination by increasing the density of the electrons and ions.

At low energies, where electron–ion recombination is less important, the S2:S1 ratio is determined by the partition of electronic stopping into initial ionization and excitation of xenon atoms. The kinematics of electronic excitation by a heavy projectile depend primarily on its velocity with respect to the target[39]. A proton with kinetic energy of 1 keV has the same velocity as a xenon atom with kinetic energy $(m_{Xe}/m_p) \times 1$ keV = 130 keV.

A recent measurement of the response of LXe to degraded alpha particles, or helium recoils, showed a partitioning that was quite xenon-like with excellent discrimination against ER[40]. As it is not fully understood what drives the partitioning between excitation and ionization for xenon recoils in LXe, it is hard to predict exactly what S2/S1 distribution hydrogen recoils might produce, but it is reasonable to take the electron recoil and xenon recoil distributions as bounding cases.

Hydrogen-doped LXe-TPC performance

Possible S1 and S2 signal losses to hydrogen. The presence of molecular species in LXe can reduce the amount of both S1 and S2 signal collected via quenching or absorption of light and charge. H_2 is not an electronegative species and should not absorb drifting electrons; the MuCap experiment operated a high pressure H_2 gas TPC at a similar H_2 density (~0.7 kg/m^3) as we hope to achieve in HydroX without seeing significant electron loss[41]. Similarly, H_2 has no absorption features near 175 nm[42], the wavelength of LXe scintillation light, as the Lyman-α series and similar excited molecular states end at ~122 nm, and the Ballmer series picks up above 360 nm[43–45].

We expect both the S1 and S2 signals to be quenched by the presence of hydrogen, but for different reasons. LXe scintillation light is produced in the decay of metastable Xe_2^* molecules formed by the combination of excited and ground state xenon atoms, $Xe^* + Xe$. The excited states, both atomic and molecular, can transfer their energy to H_2 molecules via collision, quenching the excitations before a photon is emitted, an effect observed in various combinations of GXe, LAr, and impurities like N_2, CO_2, and CH_4[46–48].

The presence of a significant concentration of molecular H_2 in the gas phase will also limit electro-luminescent amplification through a similar competition with energy transfer into molecular excitations. A simulation of the mixture of gases in the Garfield simulation package[49] suggests that adequate S2 production can be preserved for gas mixtures of over 5% percent by mole in the gas phase, and we expect that some gain can be recovered by operating at a higher amplification voltage than in the xenon-only run. A nominal operating condition for H_2 doped in LZ would be a field of 10 kV/cm in the gas phase, 25% above the current LZ operating condition, producing approximately 74 photons per electron. We generally assume that single extracted electrons will still produce enough signal to be readily detected.

Both primary scintillation and ionization signals for H_2 mole fractions up to 5.7% have been observed in a 26 atm gaseous xenon TPC for the signal from ^{241}Am 5.5 MeV alpha particles[50], with 50% losses in both channels reported for an H_2 mole fraction of 1.1%. As dual phase LXe-TPCs require the achievement of impurity levels about 20 times more stringent than achieved in ref. 50, both of the reported losses might be reduced at higher purity. The amount of H_2 that can be practically dissolved in the LXe is addressed further in the "Dissolving hydrogen in LXe" subsection of "Methods."

An accurate calibration of S1 yields vs liquid H_2 concentration may enable a precise in situ measurement of H_2 loading in a LXe-TPC with standard internal calibration sources, a silver lining that would partly offset the loss of S1 signal.

Finally, it is worth pondering on how electron transport properties are modified by doping, as this may affect the primary and additional science cases of these experiments. Estimates using ab initio calculations for molecular solutes in liquid xenon[51] confirm the cooling of drifting electrons relative to the pure liquid: the addition of molecular hydrogen increases the drift velocity by a factor of ~2 for percent-level doping, while reducing the longitudinal diffusion constant also by a factor of ~2 (Boyle, G. J. personal communication). Together, these enable sharper S2 pulses, leading to better clustering of small S2 signals and improved multiple-scatter resolution. The latter is an important parameter to discriminate γ-ray backgrounds in neutrinoless double-beta decay searches, which will be prototyped in LZ and constitute a key science case for future searches such as XLZD[52]. The faster electron drift is itself useful as it reduces accidental coincidence backgrounds, as discussed later.

Technical feasibility. A LXe-TPC should maintain high voltage and light collection performance in the presence of H_2. The S1 and S2 light signals in H_2-doped LXe will be at the same wavelength as in pure LXe, because energy will transfer from recoiling protons to xenon atoms and electrons. Over longer time scales, it is well known that PMTs can be damaged by exposure to helium and other light gases, which can diffuse through the PMT glass and cause afterpulsing (e.g., in ref. 53). The permeabilities of He, H_2, and D_2 in fused silica glass have been well measured at temperatures above room temperature[54–60], and H_2 (and D_2) mobility is slower relative to helium because of its 10% larger kinetic diameter[61]. Mechanical diffusion of all species is exponentially suppressed with decreasing temperature according to the Arrhenius equation,

$$K = K_0 \exp(-\Delta H/RT), \tag{2}$$

as less thermal energy is available to open pathways (one reason why very few measurements exist below 0 °C). Here, K is the permeability, K_0 is a reference permeability at a particular temperature, ΔH is the enthalpy of activation of the glass, R is the ideal gas constant, and T is the temperature. Based on the existing data extrapolated to lower temperatures, exposure to an atmosphere of H_2 at liquid xenon temperatures does not pose a significant risk to PMTs for run durations small compared to 80 years.

The cryogenic implications of hydrogen doping will be the major technical challenge for any implementation of HydroX. LZ has an extensive xenon handling system to circulate xenon at 400 slpm through a getter to meet the strict electronegative impurity requirements of LXe-TPCs, and the existing circulation geometry does not easily allow for the presence of a non-condensible gas in the system[62]. To mitigate this problem, our initial approach is to introduce additional stages to the circulation system to remove H_2 from the process before the xenon enters the purifier and then re-inject H_2 into the liquefied xenon as it returns to the detector. Possible methods for separation include distillation, sparging, or membrane separation[63,64]. For example, based on preliminary calculations with the McCabe–Thiele method[65], a distillation column with about 50 stages and a reflux ratio of 6.5 would be able to purify the xenon to a level where it could be recirculated for a year while building up less than 1 g of H_2 in the existing LZ getter. In the field, the DarkSide-50 experiment operated a 58 stage column to purify underground argon at Fermilab[66,67], while XENON has operated an online distillation column to remove Rn, Ar, and Kr impurities[68,69]. The extracted H_2 gas would then be re-injected into the liquid xenon using a membrane as the liquid re-enters the central TPC, maintaining a constant H_2 partial pressure head above in the gas phase above. Significant R&D on the circulation system will be required before implementation on a system of sufficient scale to be representative of a large detector.

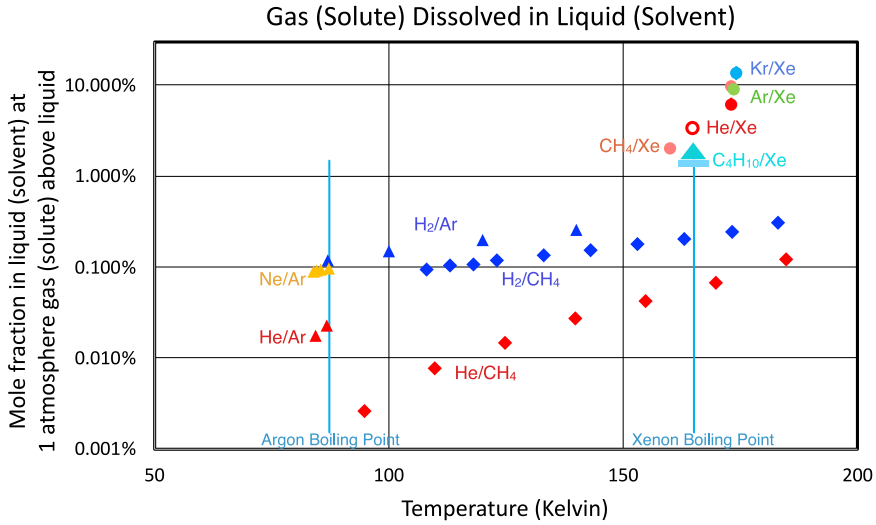

Fig. 2 | Solubilities of various gases in cold liquids as a function of temperature. Methane (argon/xenon) as a solvent are shown in diamonds (triangles/circles). The various solutes are labeled and distinguished by color. The open red circle shows unpublished data from a test stand at Fermilab. The solubilities in liquid xenon measured by LUX and associated small setups are substantially higher than those in methane and argon.

Dissolving hydrogen in LXe

The sensitivity for HydroX depends directly on the amount of H_2 that can be dissolved into the LXe. Small concentrations in the LXe mixture are governed by Henry's law: the concentration in liquid is proportional to the vapor pressure of the solute gas introduced above the LXe. We estimate Henry's coefficient based primarily on the scaling of LUX measurements of the concentrations of helium, argon, and krypton in the gas and liquid phases of xenon at 173 K for a xenon vapor pressure of 1.56 atm.

Figure 2 shows the solubilities of several mixtures[70–74], including unpublished measurements from LUX and at a test stand at Fermilab. The test stand measurements give a factor of two smaller liquid concentration than the LUX value, a difference that results in part from different temperature conditions. Xenon is substantially more efficient as a solvent than other noble gases, a consequence of the deeper Van der Waals potential[75,76]. In particular, the equilibrium concentration of H_2 (or D_2) is likely to exceed that of helium: increased solubility of a gas in a liquid is strongly correlated with a larger minimum in the Van der Waals potential[77], and the depth of the minimum in the H_2-Xe potential of 8.0 meV[78] is more than three times that of the He-Xe potential[79]. While these considerations suggest that HydroX can achieve adequate H_2 loading, no measurements of H_2 solubility in LXe currently exist, and a careful characterization of the solubilities in LXe of H_2 will be required to understand the ultimate sensitivity of HydroX.

Results and discussion

Backgrounds

By using LZ as the "host" detector, the H_2 target benefits from the exquisite low background environment of LZ, including the self-shielding provided by a large LXe mass and *xyz* reconstruction. For self-shielding: consider an external 1 MeV γ-ray entering the detector, which can Compton scatter and cause a background to a WIMP signal. This γ-ray has an attenuation length of about 6 cm in LXe, which is less than 1/10 of the 75 cm radius of LZ. The attenuation length of that same γ-ray would be 80 times the radius of a 1 m^3 high-pressure gas TPC. The attenuation length for the same γ-ray in a hypothetical 2 kg liquid hydrogen detector would be 6 times its radius. For very low energy depositions like the ones relevant for light WIMP searches, events near detector surfaces can produce significant and difficult to understand backgrounds. For example, the CoGeNT detector observed an increasing spectrum at threshold that has been interpreted as both a DM signal but also as a poorly modeled surface background[80,81]. Similar unknown sources of noise are contributing backgrounds to the new wave of ultra-low threshold detectors like SENSEI and SuperCDMS-HVeV[19,20]. For a hydrogen run in LXe-TPCs, surface effects will be suppressed by the *xyz* reconstruction, allowing the definition of a central fiducial mass where surface backgrounds are greatly reduced.

Backgrounds can be introduced with H_2 or D_2, particularly due to tritium contamination; to actually deploy H_2 in a low background environment, a tritium relative abundance less than about 1 in 10^{24} must be achieved, while atmospheric-derived sources of H_2 or D_2 have tritium concentrations at the 1 in 10^{18} level. Two potential solutions to this problem exist. First, distillation can be used to separate tritium from H_2. As one example, the MuCap experiment achieved a suppression of deuterium in hydrogen by about four orders of magnitude[82,83]; tritium would be more readily suppressed, but work remains to prove this is feasible. A second solution is an underground source of hydrogen, an area of active research for the hydrogen energy industry (e.g., ref. 84). Solvents used in low-background organic scintillators source some of their materials from underground sources, and underground argon has become a key component in rare event searches[85,86]. We do not know of any explicit measurements of the tritium content from underground sources of hydrogen, but factors of 10–100 suppression do not sound implausible.

In the sensitivity projections discussed in the next section, we take the background model used in ref. 87, with all numbers identical to those in Table III of that reference. We assume tritium can be removed by distillation or underground sources and the hydrogen brings in no other backgrounds. We do not currently assume any accidental backgrounds as observed in recent LXe-TPC detectors; more discussion on this point can be found in the next section.

WIMP sensitivity

To put everything together and calculate the DM sensitivity that could be achieved by HydroX, the SRIM hydrogen recoil model is incorporated into NEST and combined with the LZ detector model used in ref. 87 to generate a prediction for the energy threshold for H recoils in a doped LZ detector, shown in Fig. 3. Based on the high energy alpha data, the NEST model assumes that the S2/S1 splitting is similar to that of ER. We assume a loss of 50% of the generated S1 signal to quenching based on ref. 50 and S2 yields of 240 phd/e following the Garfield model above. We assume 0.95 kg of H_2 in the fiducial volume (containing 5.6 tonnes of Xe), for a mole fraction of 1.1%. The threshold is calculated for a standard S1/S2 analysis, which requires the detection of an S1 signal in at least 3 PMTs as described in ref. 87.

Figure 4 shows simulated S1/S2 distributions for hydrogen scattering from a 1 GeV WIMP, xenon nuclei scattering from ^{8}B neutrinos (similar to a ~6 GeV WIMP scattering with xenon), and the ^{214}Pb beta background. As hydrogen has only one nucleon and no neutrons, its coherent neutrino-nucleus scattering cross section is negligible compared to xenon. The H-recoil spectrum falls below the beta background because it is primarily populated by events with upward fluctuations in S1 and downward

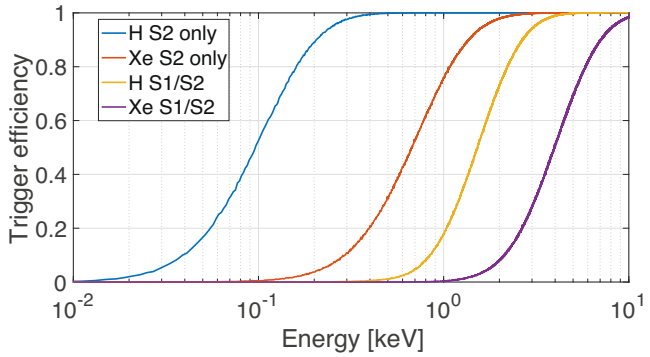

Fig. 3 | Simulated energy thresholds for Xe and H recoils in LXe. The thresholds are calculated using NEST and the full detector simulation described in ref. 87 and shown for both a standard S1/S2 analysis, requiring an S1 signal in 3 photomultiplier tubes, as well as for an S2-only analysis, requiring 3 detected electrons.

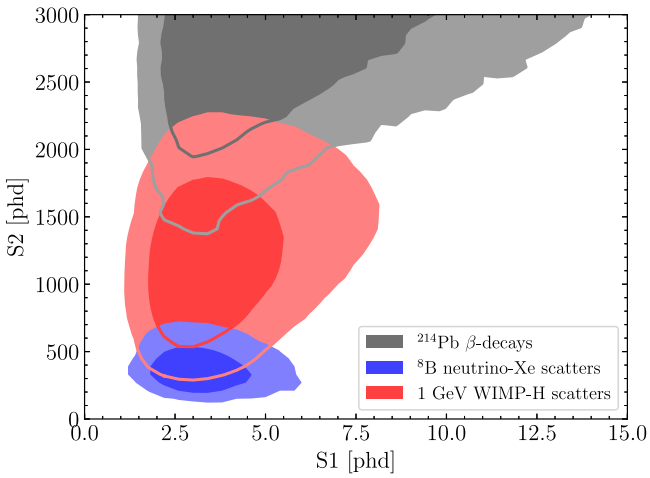

Fig. 4 | Simulated contours of S1 and S2 for various event types. The red contours show 1 GeV WIMP-hydrogen scattering, and the blue contours show ^{8}B neutrino–xenon scattering. The gray contours show ^{214}Pb beta decay events. The dark (light) region represent the 1σ (2σ) region.

fluctuations in S2 (a similar argument applies for the ^{8}B spectrum compared to a xenon recoil band or a higher energy WIMP–xenon spectrum).

LXe-TPCs provide the capability for "S2-only" analyses down to very low thresholds, as pioneered by the XENON collaborations and the DarkSide-50 experiment in liquid argon[66,88–92]. Because LXe-TPCs are sensitive to single electrons, S2-only analyses can probe energy thresholds of a few hundred eV for NR. Given the increased signal yields expected from H recoils in LXe, S2-only searches could be even more effective in a doped detector. Like other ultra-low-threshold experiments, S2-only searches give up their primary discrimination mechanism in pushing to lower energies. We calculate the sensitivity of HydroX in an S2-only analysis for two cases where we assume the analysis threshold to be either 3 electrons or 5 electrons.

The detector response to hydrogen recoils is incorporated into the same background model and Profile Likelihood Ratio analysis used in ref. 87. Figure 5 shows the projected sensitivity of a 500-day exposure for an S1/S2 analysis and the two S2-only analysis cases. The S1/S2 analysis provides competitive sensitivity down to 200 MeV, while the S2-only analysis has the potential to provide access to masses well below 100 MeV. The right panel of Fig. 5 shows the SD sensitivity of hydrogen in LZ for the same assumptions, providing unique reach to SD interactions of low mass DM particles.

Because low mass DM produces an energy spectrum that is sharply rising at the lowest energies, the sensitivity depends critically on the exact details of the detector threshold, which can only be estimated here. Therefore, these projections should be taken as merely indicative of the potential reach of HydroX. For a sense of scale, if the S1 signal is a factor of two smaller, the S1/S2 sensitivity decreases by a factor of about 3.5–4. If the amount of signal quenching forces us to use a lower loading fraction, the sensitivity would scale approximately linearly with the amount of H_2 in the detector, given the same threshold performance. The overall projected sensitivity is not dependent on the size of the S2 signal (often called "g_2"), as long as single electron resolution is maintained.

With the assumptions given, the dominant background is from ^{214}Pb decays coming from radon emanation, as it is in the higher mass searches already published by LZ. As can be seen in Fig. 4, there is not a high degree of overlap between ^{214}Pb decays and a very low mass DM signal, so the projections are not very sensitive to the exact level of ^{214}Pb in the detector. A similar argument would apply to tritium contamination, which would be more of an issue for the sensitivity of any continuing DM search with xenon recoils carried out during a HydroX run. However, this analysis does not

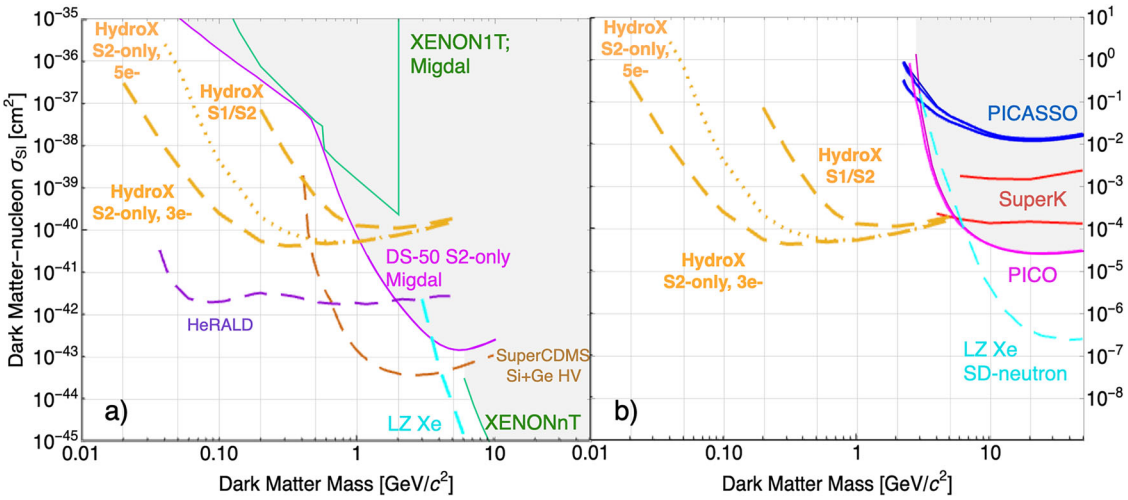

Fig. 5 | Projected sensitivity of HydroX. The dark matter reach of a 500-day run of LZ doped with H_2 under three different analysis assumptions discussed in the "WIMP Sensitivity" subsection of the "Results and discussion" is shown by the orange lines. **a** compares the sensitivity with SI projections from other existing and proposed experiments[7,22,23,87,90,94,95], while **b** compares to other SD DM–proton interactions, where there are no other sensitive experiments at low DM masses; a recent NEWS-G result is just above the plot, and we also show the LZ SD-neutron sensitivity for comparison[87,96–99]. The sensitivity of HydroX per nucleon is the same for SI and SD-proton interactions, and extends well below 100 MeV in mass.

include "accidental" events where spurious S1 and S2-only signals align in time to form a fake signal; along with the exact threshold behavior, this class of event is likely to be the true driver of the ultimate sensitivity. LZ has published results that would observe ~5 accidentals counts in this energy range over a 500-day exposure at a more conservative S2-threshold[6], which would produce a factor of ~5 reduction in the sensitivity of the S1/S2 analysis. We would likely gain some spectral discrimination against accidentals for very low mass DM but a detailed study has not been carried out. The XENON and PandaX collaborations have worked to accurately model accidental backgrounds at very low energies in the context of ^{8}B neutrino searches[92,93]. We note that S2-only backgrounds can be highly variable, depending on detector properties such as radiogenic plateout and grid emission. As S2-only backgrounds are not considered in any detail here beyond imposing an S2 threshold, the S2-only sensitivities in particular should be viewed as speculative.

Figure 5 assumes the signal would be "ER-like." If instead the signals are more "xenon-recoil-like" as indicated by ref. 40, the increase in S1 would improve sensitivity of the S1/S2 analysis by up to a factor of two in lower mass due to lower thresholds. While the experiment would gain by additional background rejection to ER events, the dominant background would become ^{8}B neutrinos scattering with xenon atoms, with significant overlap to WIMP-H scattering in the low energy regime. In particular, the ^{8}B signal would come from interactions with the full active volume of xenon, and it is likely that the absolute sensitivity in cross section would degrade.

Substitution of deuterium for hydrogen, for the same assumptions, would lead to SI sensitivities that are improved by a factor 4 albeit toward higher masses by a factor of $\sqrt{2}$. Deuterium would allow access to SD DM–neutron interactions, with sensitivities comparable to the right panel of Fig. 5, also shifted toward higher masses by the factor of $\sqrt{2}$.

Conclusion

We describe HydroX, a proposal to add hydrogen to liquid xenon time projection chambers to improve their sensitivity to low mass DM particles interacting via both SI and SD interactions. Based on assumptions about the potential signal yields for proton recoils in liquid xenon, the amount of hydrogen that can be added to the liquid, and backgrounds, a potential sensitivity is presented with interesting reach, particularly in the SD channel. There are ongoing R&D efforts to understand several of the technical challenges required to implement HydroX in a real system, and the projections presented here should be taken as merely indicative of the potential reach of HydroX.

Data availability

The data that support the findings of this study are available from the corresponding author upon reasonable request.

Received: 14 January 2025; Accepted: 1 June 2025;
Published online: 11 June 2025

References

1. Bertone, G., Hooper, D. & Silk, J. Particle dark matter: evidence, candidates and constraints. *Phys. Rept.* **405**, 279–390 (2005).
2. Feng, J. L. Dark matter candidates from particle physics and methods of detection. *Ann. Rev. Astron. Astrophys.* **48**, 495–545 (2010).
3. Jungman, G., Kamionkowski, M. & Griest, K. Supersymmetric dark matter. *Phys. Rept.* **267**, 195–373 (1996).
4. Fitzpatrick, A. L., Haxton, W., Katz, E., Lubbers, N. & Xu, Y. The effective field theory of dark matter direct detection. *J. Cosmol. Astropart. Phys.* **2013**, 004 (2013).
5. Gluscevic, V., Gresham, M. I., McDermott, S. D., Peter, A. H. G. & Zurek, K. M. Identifying the theory of dark matter with direct detection. *J. Cosmol. Astropart. Phys.* **1512**, 057 (2015).
6. Aalbers, J. et al. First dark matter search results from the LUX-ZEPLIN (LZ) experiment. *Phys. Rev. Lett.* **131**, 041002 (2023).
7. Aprile, E. et al. First dark matter search with nuclear recoils from the XENONnT experiment. *Phys. Rev. Lett.* **131**, 041003 (2023).
8. Meng, Y. et al. Dark matter search results from the PandaX-4T commissioning run. *Phys. Rev. Lett.* **127**, 261802 (2021).
9. Kozaczuk, J. & Profumo, S. Light NMSSM neutralino dark matter in the wake of CDMS II and a 126 GeV Higgs boson. *Phys. Rev.* **D89**, 095012 (2014).
10. Cerdeno, D. G., Huh, J.-H., Peiro, M. & Seto, O. Very light right-handed sneutrino dark matter in the NMSSM. *J. Cosmol. Astropart. Phys.* **1111**, 027 (2011).
11. Lin, T., Yu, H.-B. & Zurek, K. M. On symmetric and asymmetric light dark matter. *Phys. Rev.* **D85**, 063503 (2012).
12. Battaglieri, M. et al. US cosmic visions: new ideas in dark matter 2017: community report. http://lss.fnal.gov/archive/2017/conf/fermilab-conf-17-282-ae-ppd-t.pdf (2017).
13. High Energy Physics, U.S. Department of Energy. *Basic Research Needs for Dark Matter Small New Initiatives*. Technical Report. https://science.energy.gov/media/hep/pdf/Reports/Dark_Matter_New_Initiatives_rpt.pdf (2019).
14. Cooley, J. et al. Report of the Topical Group on Particle Dark Matter for Snowmass. Preprint at https://arxiv.org/abs/2209.07426 (2022).
15. Akerib, D. S. et al. Snowmass2021 cosmic frontier dark matter direct detection to the neutrino fog. Preprint at https://arxiv.org/abs/2203.08084 (2022).
16. Essig, R. et al. Snowmass2021 cosmic frontier: the landscape of low-threshold dark matter direct detection in the next decade. Preprint at https://arxiv.org/abs/2203.08297 (2022).
17. Arnaud, Q. et al. First results from the NEWS-G direct dark matter search experiment at the LSM. *Astropart. Phys.* **97**, 54–62 (2018).
18. Aguilar-Arevalo, A. et al. Constraints on light dark matter particles interacting with electrons from DAMIC at SNOLAB. *Phys. Rev. Lett.* **123**, 181802 (2019).
19. Abramoff, O. et al. SENSEI: direct-detection constraints on sub-GeV dark matter from a shallow underground run using a prototype skipper-CCD. *Phys. Rev. Lett.* **122**, 161801 (2019).
20. Agnese, R. et al. First dark matter constraints from a SuperCDMS single-charge sensitive detector. *Phys. Rev. Lett.* **121**, 051301 (2018); erratum *Phys. Rev. Lett.* **122**, 069901 (2019).
21. Aalbers, J. et al. Search for new physics in low-energy electron recoils from the first LZ exposure. *Phys. Rev. D* **108**, 072006 (2023).
22. Aprile, E. et al. Search for light dark matter interactions enhanced by the Migdal effect or Bremsstrahlung in XENON1T. *Phys. Rev. Lett.* **123**, 241803 (2019).
23. Agnes, P. et al. Search for dark-matter–nucleon interactions via Migdal effect with DarkSide-50. *Phys. Rev. Lett.* **130**, 101001 (2023).
24. Akerib, D. S. et al. The LUX-ZEPLIN (LZ) experiment. *Nucl. Instrum. Methods* **A953**, 163047 (2020).
25. Aalbers, J. et al. A next-generation liquid xenon observatory for dark matter and neutrino physics. *J. Phys. G* **50**, 013001 (2023).
26. Aalbers, J. et al. The XLZD Design Book: towards the Next-generation Liquid Xenon Observatory for dark matter and neutrino physics. Preprint at https://arxiv.org/abs/2410.17137 (2024).
27. Akerib, D. S. et al. The LUX-ZEPLIN (LZ) radioactivity and cleanliness control programs. *Eur. Phys. J. C* **80**, 1044 (2020); erratum *Eur. Phys. J. C* **82**, 221 (2022).
28. Szydagis, M. et al. NEST: a comprehensive model for scintillation yield in liquid xenon. *J. Instrum.* **6**, P10002 (2011).
29. Szydagis, M., Fyhrie, A., Thorngren, D. & Tripathi, M. Enhancement of NEST capabilities for simulating low-energy recoils in liquid xenon. *J. Instrum.* **8**, C10003 (2013).
30. Szydagis, M. et al. Noble element simulation technique v2.0. Zenodo https://zenodo.org/records/1314669 (2019).
31. Fermi, E. *A Course in Neutron Physics, Part 1*. Technical Report. LADC-225, Los Alamos National Laboratory Notes by I. Halpern (Atomic Energy Commission, 1946).

32. Segrè, E. in *Nuclei and Particles* 621–626 (W.A. Benjamin, Inc., 1977).
33. Krstić, P. S. & Schultz, D. R. Elastic and related transport cross sections for protons scattering from the noble gases He, Ne, Ar, Kr, and Xe. *Phys. Plasma* **13**, 053501 (2006).
34. Zielger, J. F., Biersack, J. P. & Littmark, J. *The Stopping and Range of Ions in Solids* (Pergamon Press, Inc., 1985).
35. Ziegler, J. F., Ziegler, M. & Biersack, J. SRIM - The stopping and range of ions in matter (2010). *Nucl. Instrum. Methods* **B268**, 1818–1823 (2010).
36. Dahl, C. E. *The Physics of Background Discrimination in Liquid Xenon, and First Results from Xenon10 in the Hunt for WIMP Dark Matter*. PhD thesis, Princeton Univ. (2009).
37. Bradley, A. W. *LUX Thermosyphon Cryogenics and Radon-Related Backgrounds for the First WIMP Result*. PhD thesis, Case Western Reserve Univ. (2014).
38. Rischbieter, G. NEST v2: a comprehensive model for scintillation and ionization in noble elements. CPAD 2018, University of New Mexico, Albuquerque, NM, USA. https://indico.fnal.gov/event/18104/contributions/45879/attachments/28566/35314/CPAD_NESTv2_GR_2.pdf (2018).
39. Fermi, E. & Teller, E. The capture of negative mesotrons in matter. *Phys. Rev.* **72**, 399–408 (1947).
40. Haselschwardt, S. J. et al. First measurement of discrimination between helium and electron recoils in liquid xenon for low-mass dark matter searches. *Phys. Rev. Lett.* **132**, 111801 (2024).
41. Egger, J. et al. A high-pressure hydrogen time projection chamber for the MuCap experiment. *Eur. Phys. J.* **A50**, 163 (2014).
42. Fujii, K. et al. High-accuracy measurement of the emission spectrum of liquid xenon in the vacuum ultraviolet region. *Nucl. Instrum. Methods A* **795**, 293–297 (2015).
43. Herzberg, G. *Molecular Spectra and Molecular Structure, Vol I: Spectra of Diatomic Molecules* 2nd edn (D Van Nostrand Co., 1950).
44. Keller-Rudek, H., Moortgat, G. K., Sander, R. & Sorensen, R. The mpi-mainz uv/vis spectral atlas of gaseous molecules of atmospheric interest. *Earth Syst. Sci. Data* **5**, 365–373 (2013).
45. Shaw, G., Ferland, G. J., Abel, N. P., Stancil, P. C. & van Hoof, P. A. M. Molecular hydrogen in star-forming regions: implementation of its micro-physics in cloudy. *Astrophys. J.* **624**, 794–807 (2005).
46. Acciarri, R. et al. Effects of nitrogen contamination in liquid argon. *J. Instrum.* **5**, P06003 (2010).
47. Pushkin, K. et al. A scintillation response and an ionization yield in pure xenon and mixtures of it with methane. *Instrum. Exp. Tech.* **49**, 489–493 (2006).
48. Henriques, C. A. O. et al. Secondary scintillation yield of xenon with sub-percent levels of CO_2 additive for rare-event detection. *Phys. Lett.* **B773**, 663–671 (2017).
49. Veenhof, R. in *Programming And Mathematical Techniques In Physics - Proceedings Of The Conference On Programming And Mathematical Methods For Solving Physical Problems* 66–71 (World Scientific, 1993).
50. Tezuka, C. et al. Electron diffusion and scintillation in xenon doped with hydrogen for high-pressure xenon time projection chamber. In *Proc. 2004 IEEE Nuclear Science Symposium and Medical Imaging Conference (NSS/MIC 2004)* 1157–1159 (IEEE, 2004).
51. Boyle, G. J. et al. Electron scattering and transport in simple liquid mixtures. *J. Phys. B Atomic Mol. Opt. Phys.* **57**, 015202 (2024).
52. Aalbers, J. et al. Neutrinoless double beta decay sensitivity of the XLZD rare event observatory. *J. Phys. G Nucl. Part. Phys.* **52**, 045102 (2024).
53. Incandela, J. R. et al. The performance of photomultipliers exposed to helium. *Nucl. Instrum. Methods* **A269**, 237–245 (1988).
54. Norton, F. J. Helium diffusion through glass. *J. Am. Ceram. Soc.* **36**, 90–96 (1953).
55. Altemose, V. O. Helium diffusion through glass. *J. Appl. Phys.* **32**, 1309–1316 (1961).
56. Swets, D. E., Lee, R. W. & Frank, R. C. Diffusion coefficients of helium in fused quartz. *J. Chem. Phys.* **34**, 17–22 (1961).
57. Lee, R. W., Frank, R. C. & Swets, D. E. Diffusion of hydrogen and deuterium in fused quartz. *J. Chem. Phys.* **36**, 1062–1071 (1962).
58. Lee, R. W. Diffusion of hydrogen in natural and synthetic fused quartz. *J. Chem. Phys.* **38**, 448–455 (1963).
59. Shelby, J. E. Molecular diffusion and solubility of hydrogen isotopes in vitreous silica. *J. Appl. Phys.* **48**, 3387–3394 (1977).
60. Williams, G. A. & Ferguson, J. B. The diffusion of hydrogen and helium through silica glass and other glasses. *J. Am. Chem. Soc.* **44**, 2160–2167 (1922).
61. Mehio, N., Dai, S. & Jiang, D.-e Quantum mechanical basis for kinetic diameters of small gaseous molecules. *J. Phys. Chem.* **A118**, 1150–1154 (2014).
62. Jensen, M. K. in *Two-Phase Flow Heat Exchangers* (eds Kakac, S., Bergles, A. & Fernandes, E. O.) Ch. 10 (Kluwer Academic Publishers, 1988).
63. Adhikari, S. & Fernando, S. Hydrogen membrane separation techniques. *Ind. Eng. Chem. Res.* **45**, 875–881 (2006).
64. Li, J. et al. Efficient electrocatalytic CO_2 reduction on a three-phase interface. *Nat. Catal.* **1**, 592–600 (2018).
65. McCabe, W. L., Smith, J. C. & Harriott, P. *Unit Operations of Chemical Engineering* 7th edn (McGraw-Hill, 2005).
66. Agnes, P. et al. DarkSide-50 532-day dark matter search with low-radioactivity argon. *Phys. Rev.* **D98**, 102006 (2018).
67. Back, H. O. et al. First commissioning of a cryogenic distillation column for low radioactivity underground argon. Preprint at https://arxiv.org/abs/1204.6061 (2012).
68. Aprile, E. et al. Online ^{222}Rn removal by cryogenic distillation in the XENON100 experiment. *Eur. Phys. J. C* **77**, 358 (2017).
69. Aprile, E. et al. Application and modeling of an online distillation method to reduce krypton and argon in XENON1T. *Prog. Theor. Exp. Phys.* **2022**, 053H01 (2022).
70. Karasz, F. E. & Halsey, G. D. Solubility of helium and neon in liquid argon. An approximation to the entropy of lattice vacancy formation in liquid argon. *J. Chem. Phys.* **29**, 173–179 (1958).
71. Volk, H. & Halsey, G. D. Solubility of hydrogen and deuterium in liquid argon. *J. Chem. Phys.* **33**, 1132–1139 (1960).
72. Heck, C. K. & Hiza, M. J. Liquid-vapor equilibrium in the system helium-methane. *AIChE J.* **13**, 593–599 (1967).
73. Shukla, K. P. & Lucas, K. Prediction of gas solubility henry coefficients in simple systems. *Fluid Phase Equilib.* **28**, 211–216 (1986).
74. Yoshino, K., Sowada, U. & Schmidt, W. F. Effect of molecular solutes on the electron drift velocity in liquid Ar, Kr, and Xe. *Phys. Rev. A* **A 14**, 438–444 (1976).
75. Pollack, G. L. Why gases dissolve in liquids. *Science* **251**, 1323–1330 (1991).
76. Rentzepis, P. M. & Douglass, D. C. Xenon as a solvent. *Nature* **293**, 165–166 (1981).
77. Prausnitz, J. M., Lichtenthaler, R. N. & de Azevedo, E. G. *Molecular Thermodynamics of Fluid-Phase Equilibria* 2nd edn (Prentice-Hall Inc., 1986).
78. Le Roy, R. J. & Hutson, J. M. Improved potential energy surfaces for the interaction of H_2 with Ar, Kr, and Xe. *J. Chem. Phys.* **86**, 837–853 (1987).
79. Danielson, L. J. & Keil, M. Interatomic potentials for HeAr, HeKr, and HeXe from multiproperty fits. *J. Chem. Phys.* **88**, 851–870 (1988).
80. Aalseth, C. E. et al. Maximum likelihood signal extraction method applied to 3.4 years of cogent data. Preprint at https://arxiv.org/abs/1401.6234 (2015).
81. Aalseth, C. E. et al. CoGeNT: a search for low-mass dark matter using p-type point contact germanium detectors. *Phys. Rev.* **D88**, 012002 (2013).

82. Andreev, V. A. et al. Measurement of muon capture on the proton to 1% precision and determination of the pseudoscalar coupling g_P. *Phys. Rev. Lett.* **110**, 012504 (2013).
83. Alekseev, I. et al. Hydrogen distallation at the deuterium removal unit of mucap experiment. Tech. Rep. PNPI-2702, Petersburg Nuclear Physics Institute, Gatchina 188350, Russia. https://muon.npl.washington.edu/twiki/pub/MuCap/CryoDestillation/DRU-NHA-manuscript.pdf (2006).
84. Zgonnik, V. The occurrence and geoscience of natural hydrogen: a comprehensive review. *Earth Sci. Rev.* **203**, 103140 (2020).
85. Alimonti, G. et al. Measurement of the ^{14}C abundance in a low-background liquid scintillator. *Phys. Lett. B* **422**, 349–358 (1998).
86. Agnes, P. et al. Results from the first use of low radioactivity argon in a dark matter search. *Phys. Rev. D* **93**, 081101 (2016); addendum *Phys. Rev. D* **95**, 069901 (2017).
87. Akerib, D. S. et al. Projected WIMP sensitivity of the LUX-ZEPLIN dark matter experiment. *Phys. Rev. D* **101**, 052002 (2020).
88. Angle, J. et al. A search for light dark matter in XENON10 data. *Phys. Rev. Lett.* **107**, 051301 (2011).
89. Aprile, E. et al. Low-mass dark matter search using ionization signals in XENON100. *Phys. Rev.* **D94**, 092001 (2016).
90. Agnes, P. et al. Low-mass dark matter search with the DarkSide-50 experiment. *Phys. Rev. Lett.* **121**, 081307 (2018).
91. Aprile, E. et al. Search for light dark matter in low-energy ionization signals from XENONnT. *Phys. Rev. Lett.* **134**, 161004 (2025).
92. Bo, Z. et al. First measurement of solar ^8B neutrino flux through coherent elastic neutrino-nucleus scattering in PandaX-4T. *Phys. Rev. Lett*. **133**, 191001 (2024).
93. Aprile, E. et al. First measurement of solar ^8B neutrinos via coherent elastic neutrino-nucleus scattering with XENONnT. *Phys. Rev. Lett*. **133**, 191002 (2024).
94. Hertel, S. A., Biekert, A., Lin, J., Velan, V. & McKinsey, D. N. Direct detection of sub-GeV dark matter using a superfluid ^4He target. *Phys. Rev. D* **100**, 092007 (2019).
95. Agnese, R. et al. Projected sensitivity of the SuperCDMS SNOLAB experiment. *Phys. Rev.* **D95**, 082002 (2017).
96. Amole, C. et al. Dark matter search results from the complete exposure of the PICO-60 C_3F_8 bubble chamber. *Phys. Rev.* **D100**, 022001 (2019).
97. Behnke, E. et al. Final results of the PICASSO dark matter search experiment. *Astropart. Phys.* **90**, 85–92 (2017).
98. Choi, K. et al. Search for neutrinos from annihilation of captured low-mass dark matter particles in the Sun by Super-Kamiokande. *Phys. Rev. Lett.* **114**, 141301 (2015).
99. Arora, M. M. et al. Search for light dark matter with NEWS-G at the LSM using a methane target. *Phys. Rev. Lett.***134**, 141002 (2025).

Acknowledgements

Funding for this work is supported by the U.S. Department of Energy, Office of Science, Office of High Energy Physics under Contract Numbers DE-SC0021115, DE-AC02-05CH11231, DE-SC0020216, DE-AC02-07CH11359, DE-SC0015910, DE-SC0011702, DE-SC0015708, DE-SC0008475, DE-SC0013542, DE-AC02-76SF00515, and DE-SC0019066.

Author contributions

The content of this article was developed in part from the narratives of experiment proposals led by W. H. Lippincott and H. N. Nelson, involving many of the authors. All authors iterated on the original proposals and approved the final version of the manuscript.

Competing interests

The authors declare no competing interests.

Additional information

Correspondence and requests for materials should be addressed to W. H. Lippincott.

Peer review information *Communications Physics* thanks Ettore Segreto and the other anonymous reviewer(s) for their contribution to the peer review of this work.